4. Shen, H., Perrie, W. and He, Y., A new hurricane wind retrieval algorithm for SAR images. *Geophys. Res. Lett.*, 2006, **33**(21), L21812-1–L21812-5.
5. Vachon, P. W. and Wolfe, J., C-band cross-polarization wind speed retrieval. *IEEE Geosci. Remote Sensing Lett.*, 2011, **8**(3), 456–459.
6. Hwang, P. A., Zhang, B. and Perrie, W., Depolarized radar return for breaking wave measurement and hurricane wind retrieval. *Geophys. Res. Lett.*, 2010, **37**(1), L01604-1–L01604-4.
7. Monaldo, F. M., Jackson, C. and Li, X., On the use of Sentinel-1 cross-polarization imagery for wind speed retrieval. *Int. Geosci. Remote Sensing Symp.*, 2017, 392–395.
8. Shao, W. *et al.*, Development of wind speed retrieval from cross-polarization Chinese Gaofen-3 synthetic aperture radar in typhoons. *Sensors*, 2018, **18**, 412.
9. Gao, Y. *et al.,* A wind speed retrieval model for Sentinel-1A EW mode cross-polarization images. *Remote Sensing*, 2019, **11**, 153; doi:10.3390/rs11020153.
10. Mouche, A. *et al.*, Copolarized and cross-polarized SAR measurements for high-resolution description of major hurricane wind structures: application to Irma category 5 hurricane. *J. Geophys. Res. Oceans*, 2019, **124**, 3905–3922; https://doi.org/10.1029/2019JC015056.
11. Jagdish *et al.*, An interesting case of persistent rain cells observed by RISAT-1 SAR over the Indian Ocean during a pair of depression–cyclone interactions (August, 2012). *Remote Sensing Lett.*, 2019, **10**(6), 545–552; doi:10.1080/2150704X.2019.1579377.
12. Jagdish *et al.*, Atmospheric fronts using RISAT-1 SAR data: case studies for shear lines. *IEEE J. Sel. Top. Appl. Earth Observ. Remote Sensing*, 2018, **11**(12), 4711–4717; doi:10.1109/JSTARS.2018.2878753.
13. Zhang, B. *et al*., Tropical cyclone vector winds from C-band dual-polarization synthetic aperture radar. *Int. Geosci. Remote Sensing Symp.*, 2014, 3522–3525.
14. Jiang, Z. *et al.*, A damped Newton variational inversion method for SAR wind retrieval. *J. Geophys. Res.*, 2016, **122**(2), 823–845.
15. Jagdish, Kumar, S. V. V. A., Chakraborty, A. and Kumar, R., Validation of wind speed retrieval from RISAT-1 SAR images of the North Indian Ocean. *Remote Sensing Lett*., 2018, **9**(5), 421–428; doi:10.1080/2150704X.2018.1430392.

ACKNOWLEDGEMENTS. We thank the Director, Space Applications Centre, ISRO, Ahmedabad for his encouragement. We also thank NRSC and PODAAC for providing RISAT-1 and ASCAT data respectively, and the RISAT-1 data calibration and validation team. We also thank Shri Rakesh R. Bhavsar and Shri. Deba Jyoti Dhar (Space Applications Centre, ISRO, Ahmedabad) for their valuable suggestions.

Received 12 March 2019; revised accepted 25 December 2019

doi: 10.18520/cs/v118/i8/1282-1286

Correlation between Earth tides and the 2008 M_S 8.0 Wenchuan earthquake sequence

Ruyu Yan[1], Chaodi Xie[1,2,*], Xinglin Lei[3], Han Zhang[1], Rui Jia[1] and Jianping Liao[4]

[1]Geophysics Department, School of Resources and Earth Science, Yunnan University, Kunming 650091, China
[2]State Key Laboratory of Earthquake Dynamics, Institute of Geology, China Earthquake Administration, Beijing 100029, China
[3]Geological Survey of Japan, AIST, Tsukuba 305-8567, Japan
[4]Hunan Provincial Key Laboratory of Shale Gas Resource Utilization, Hunan University of Science and Technology, Xiangtan 411201, China

This study examines the possibility of tidal triggering in the aftershock sequence of the M_S 8.0 Wenchuan earthquake on 12 May 2008. Two methods, the Schuster spectrum and KORRECT (correlation with a rectangular pulse) methods, were used to explore the periodicities of the aftershock sequence. Firstly, we detected the latent periodicities through the Schuster spectrum method; then, we used the KORRECT method to verify and confirm these periodicities. Moreover, the aftershock catalogue was divided into two subsets using 16 km focal depth to discuss the impact of focal depth on tidal triggering. Results show that the aftershocks in the first few days following the mainshock were mainly triggered by semidiurnal and diurnal tides. In the Longmen Shan Thrust Belt, shallow earthquakes were triggered by diurnal tides and deep earthquakes were triggered by semidiurnal tides.

Keywords: Aftershock, earth tides, KORRECT method, schuster spectrum, 2008 M_S 8.0 Wenchuan earthquake.

THE oceans and solid earth are periodically deformed under the forces of celestial bodies (mainly the Sun and the Moon). We usually refer to them as solid tides and ocean tides. Related research indicates that although the variation of the solid tidal stress is 10^3 Pa, which is much smaller than the average stress drop of the earthquake, the rate of accumulation is usually greater than the tectonic stress[1]. Therefore, when the pressure in the focal area is close to the critical level at which the earthquake occurs, the tides may trigger an earthquake. Studying tidal triggering can provide clues to the physical mechanisms that solve fault rupture.

Because stress changes due to the earth's tide can be predicted, some studies have studied the relationship between the earth's tide and aftershocks. Early in 1966, Berg[2] supposed that the unloading of the crust by large ocean tides may be considered a triggering mechanism for the Alaska earthquake of March 1964, and its major aftershocks. Mohler[3] considered that when tidal stress is favourable for motion on the fault plane, notable events

*For correspondence. (e-mail: xiecd@ynu.edu.cn)

are continuously triggered during the entire sequence and large integral aftershock occurs. Tanaka[4] used the Schuster test to determine that the Sumatra megathrust earthquakes and Tohoku-Oki earthquake[5] were triggered by tides. Xie[6] observed the obvious diurnal tides in the Ning'er area of the Yunnan province with the Schuster spectrum.

The Wenchuan earthquake ($M_S = 8.0$) occurred in a well-monitored zone. As a result, an almost complete record of all aftershocks of local duration magnitude $M_L \geq 2$ is available. Li and Jiang[7] and Li[8] have found Wenchuan aftershocks activity was triggered by tidal forces and have systematically studied them based on the Schuster test. Chen[9] preliminarily found tidal force triggering of the M_S 8.0 Wenchuan earthquake and its strong aftershocks by calculating azimuths, scale, and rate of change of the tidal force.

In this study, we investigate the correlation between the 2008 M_S 8.0 Wenchuan earthquake sequence and earth tides using the methods of the Schuster spectrum[10] and KORRECT[11]. Firstly, the Schuster spectrum method is used to analyse the seismic sequence in order to obtain the possible periods of aftershocks. Furthermore, the KORRECT method is used to test the significance level of the tidal periods found in the results of the Schuster spectrum. Moreover, we preliminarily discuss the characteristics of the tidal triggering effect on the M_S 8.0 Wenchuan earthquake and its aftershocks.

The M_S 8.0 Wenchuan earthquake occurred at 06:27:56.8 UT on 12 May 2008, at the Longmen Shan Fault Zone in the Sichuan province of China. The epicentre was located at 31.0°N, 103.4°E, the focal depth was 16 km and the rupture length was 330 km (ref. 12) (Table 1). Aftershock activity was very frequent. According to the data from Huang[12], by the end of 18 May 2008, the number of aftershocks was about 536. The times of these data were converted into world time in our following tidal calculations. The spatial aftershock distribution is shown in Figure 1. Figure 2 shows the depth and magnitude distributions of aftershocks.

The M_S 8.0 Wenchuan earthquake occurred in the Longmen Shan Thrust Belt on the eastern margin of the Qinghai–Tibet Plateau. The belt extends from the northeast to the southwest. As seen in Figure 1, aftershocks were mainly concentrated in the upper plate of the Beichuan–Yingxiu Fault, the lower part of the Wenchuan–Maoxian Fault and Qingchuan Fault[13–16].

Since the aftershock sequence is irregularly spaced, with no associated amplitude, routine methods are not suitable for detecting periodicities[11]. We enlisted two methods to study possible periodicities in the aftershock sequence: the Schuster spectrum and the KORRECT method.

The Schuster spectrum is popularly used in periodicity examination; it provides a way to detect any unknown periodicity in a catalogue and analyse any non-uniformity of seismicity rate[6,10,16]. The length of the sequence and the periodicity need to satisfy the equation: $\varepsilon T = t$, where t represents the length of the sequence and T represents the latent periodicity. ε determines the subset of periods at which the spectrum will be computed, and the value of ε is at least 1 (ref. 10). In this communication, we set $\varepsilon = 2$, because of the Nyquist theorem.

The KORRECT method (correlation with a rectangular pulse) not only verifies the results obtained by spectral analysis, but also provides some new details[11]. The KORRECT method is basically the correlation between the occurrence time of aftershocks and the rectangular pulse sequence in a particular period. By counting the number of aftershocks within the pulse, we obtain a 'phase variation curve', which determines the aftershock density as a function of phase at a particular period. This method was originally developed to detect triggering of aftershocks by the free oscillations of the earth[17].

Firstly, we use the Schuster spectrum to detect the latent periodicity in aftershocks; then, we use KORRECT to verify whether the obtained periodicities correspond to the tide periodicity.

We analysed the aftershocks using the Schuster spectrum and KORRECT methods. Firstly, we calculated the Schuster spectrum and phase variation curves for 0–3 days, 1–4 days, 2–5 days and 3–6 days following the mainshock (Figure 3). Periodicity becomes a significant rather than an arbitrary value when it surpasses 95% confidence[10]. The Schuster spectrum exhibits obvious semidiurnal periodicity in Figure 3 *a*, *c* and *e*, we also find a trace of diurnal periodicity in Figure 3 *a*, corresponding to the semidiurnal and diurnal components of the earth's tide.

Encouraged by the results of the Schuster spectrum, we used the KORRECT time-domain method for further verification. According to the method of KORRECT, we move one day in order to detect the periodicity clearly. In other words, the first data set starts the first day after the mainshock with a duration of three days; the second data set starts the second day after the mainshock with a duration of three days, etc. Through this method, every 3 days of aftershocks can include more than 100 aftershocks. A pulse series is used in the calculation by repeating a finite-width rectangular pulse at regular intervals. The

Table 1. Parameters for the 2008 M_S 8.0 Wenchuan earthquake

Parameters	Value
Occurrence time	2008-05-12, 14:27:56.8
Location	31.00°N, 103.34°E
M_L	8.0
Depth	16 km
Strike	247°
Dip	62°
Rake	131°
Friction	0.4

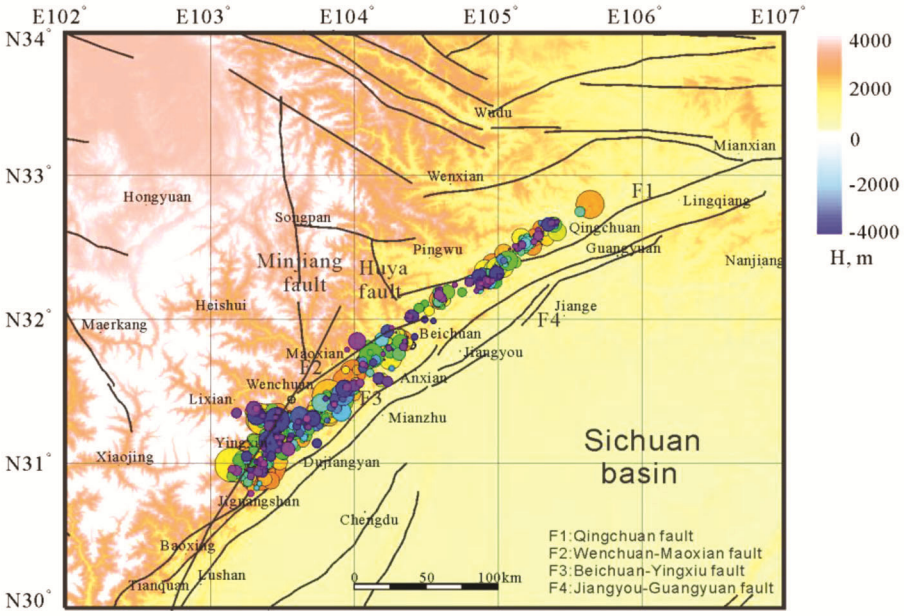

Figure 1. Distribution of Wenchuan aftershocks and the tectonic setting of the study region. The size of the circle represents the magnitude of aftershocks; the colour of the circle represents time after the mainshock, increasing through orange, green, blue and purple. The colour chart on the right side of the figure indicates elevation.

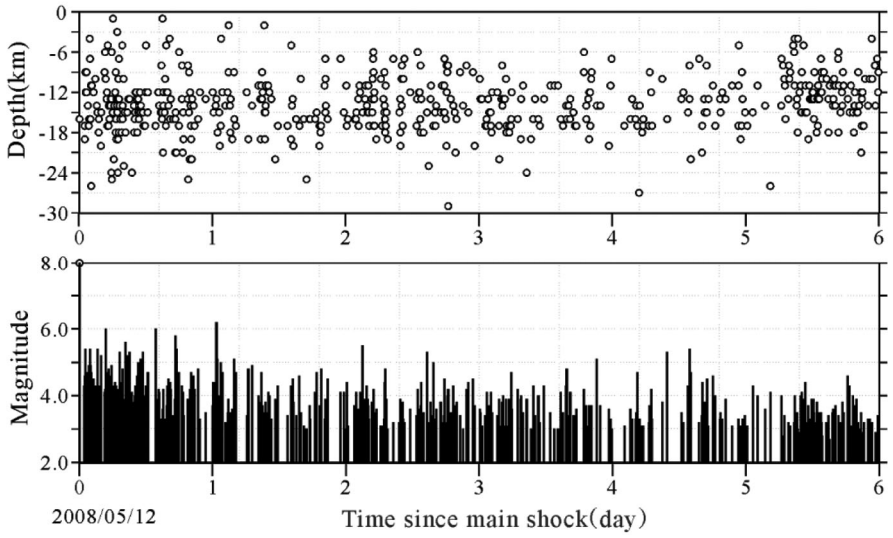

Figure 2. Depth and magnitude distributions of aftershocks.

period of the pulse series was made equal to the periods obtained in the spectral analysis.

Figure 3 *b*, *d*, *f* and *h* show the phase variation curves at a period of 0.5 days with a pulse of 0.1 days. The number of aftershocks within the pulse can be used to plot a phase variation curve, which displays aftershock density as a function of phase for a particular period. The aftershock density demonstrates cyclic behaviour with a minimum and maximum separated by about 180° in phase, similar to a sinusoidal curve. By the end of the 6th day after the mainshock, cyclic behaviours were no longer observed in the phase variation curves. These results indicate that aftershocks may mainly be triggered by semidiurnal tides.

Figure 3 *a*, *c*, *e*, and *g* do not show clear patterns of aftershock density, but Figure 3 *b*, *d*, *f* and *h* have declining trends over the semidiurnal period. By the end of the 6th day, the data lose their inherent features; therefore, we did not calculate the remaining aftershocks.

Figure 3 *a* demonstrates obvious semidiurnal and diurnal periodicity. Therefore, we further verified the 1 day period using the aftershocks between 0 and 3 days

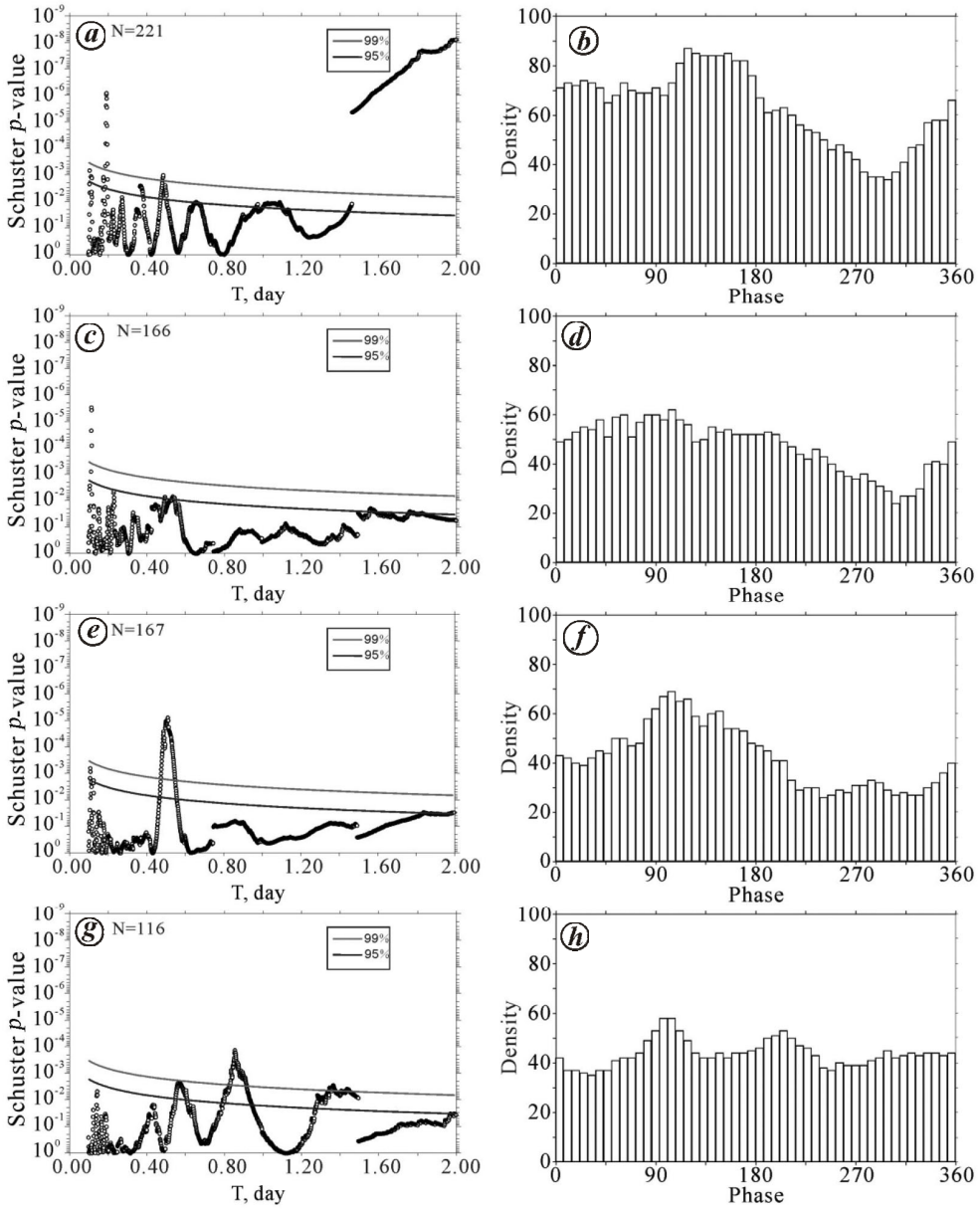

Figure 3. Schuster spectrum and phase variation curves for (***a***) 0–3 days, (***b***) 1–4 days, (***c***) 2–5 days and (***d***) 3–6 days after the mainshock.

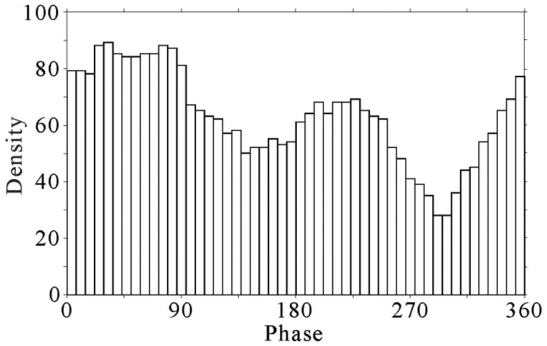

Figure 4. Phase variation curves for 0–3 days after the main shock. The period of the pulse series is 1 day and the pulse width is set to 0.2 days.

(Figure 4). The pulse width was set to 0.2 days. In this case, cyclic behaviour in the aftershock density with two minimums and two maximums was observed, which indicates that aftershocks may be triggered by diurnal tides.

Thereby, using two approaches, we find that, aftershocks in these time spans were triggered by tides, including semidiurnal and diurnal tides.

In order to test the effect of depth on tidal triggering, the data set was divided into two subsets: set A contains the shallow aftershocks ($0 \le \text{depth} < 15$ km) and set B contains deep aftershocks ($15 \le \text{depth} \le 30$ km).

We separately analysed aftershocks from 0–3 days after the mainshock in sets A and B.

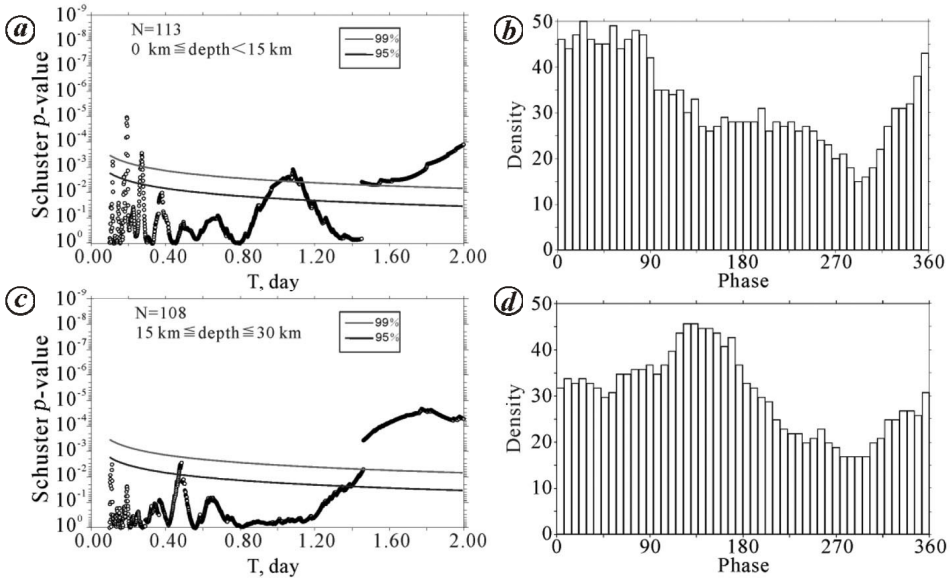

Figure 5. Schuster spectrum and phase variation curves 0–3 days after the mainshock in sets A and B.

Figure 5 *a* and *c* show the results of the Schuster spectrum. The Schuster spectrum exhibits obvious diurnal periodicity in set A (Figure 5 *a*), and obvious semidiurnal periodicity in set B (Figure 5 *c*). Figure 5 *b* and *d* show the phase variation curves corresponding to Figure 5 *a* and *c*. The phase variation curves in Figure 5 *b* have a period of 1 day with pulse width of 0.2 days; the phase variation curves in Figure 5 *d* have a period of 0.5 days with pulse width of 0.1 days. These phase variation curves show cyclic behaviour in the aftershock density, with a minimum and maximum indicating that the aftershocks at both depths may be triggered by tidal stress.

Thereby, through two analyses of two subsets of 0–3 days aftershocks, we can preliminarily conclude that the shallow aftershocks were mainly triggered by diurnal tides, and the deep aftershocks were mainly triggered by semidiurnal tides.

Compared to the increasing confining stresses on faults, tidal dilations become relatively smaller with depth[18–21]. Therefore, shallow earthquakes are more easily triggered by earth tides. But our results illustrate that aftershocks were triggered by different tides regardless of shallow or deep earthquakes.

Figures 3 *a*, 5 *a* and 5 *c* also show clear periodicity near the 2 days point with 99% confidence. In order to explore this periodicity, we expanded the duration of the data set to 5 days after the mainshock (Figure 6). Figure 6 is also used to analyse the influence of depth on the tidal triggering.

Figure 6 shows that the Schuster spectrum can exhibit obvious 2 days periodicity in all situations (Figure 6 *a*, *c* and *e*). From Figure 6, we also find that aftershocks at all depths display obvious semidiurnal periodicity (set B) and fuzzy diurnal periodicity (set A). In Figure 6 *b*, *d*, and *f*, the KORRECT method was used to obtain the corresponding phase variation curves with period of 2 days and pulse width of 0.2 days. These phase variation curves show cyclic behaviour in the aftershock density, with four minimums and four maximums. However, the earth's tide does not have a 2 days component; the 2 days period may be the double effect of diurnal tide. Therefore, aftershocks at all depths may be triggered by tidal stress.

In this study, we found that shallow earthquakes were triggered by diurnal tides and deep earthquakes were triggered by semidiurnal tides. This could be due to differences in the crustal structure and tectonic implications[21]. According to the tectonic setting in Wenchuan, as the depth of the Longmen Shan Fault (the main fault) increases, the dip of the fault decreases until the angle is nearly vertical[22]. There is a zone of low velocity and low resistivity[23,24] in the Longmen Shan Fault at the depth of 15–20 km, and due to the large amplitude of the semidiurnal tides compared with diurnal tides, it may have induced the detachment layer of the nappe tectonic belt, and thus played a more significant role in deep earthquakes. Therefore, associated aftershocks may be influenced by diurnal tides, and deep aftershocks may be influenced by semidiurnal tides.

In this study, we used the M_S 8.0 Wenchuan earthquake sequence to analyse aftershocks from 12–18 May 2008. Through the Schuster spectrum and KORRECT methods, it is evident that the earth tides had strong influence on the occurrence times of aftershocks of the 2008 M_S 8.0 Wenchuan earthquake, and the aftershocks during the first few days were triggered by semidiurnal and diurnal tides. Moreover, we divided the aftershock catalogue into two subsets and concluded that shallow earthquakes were

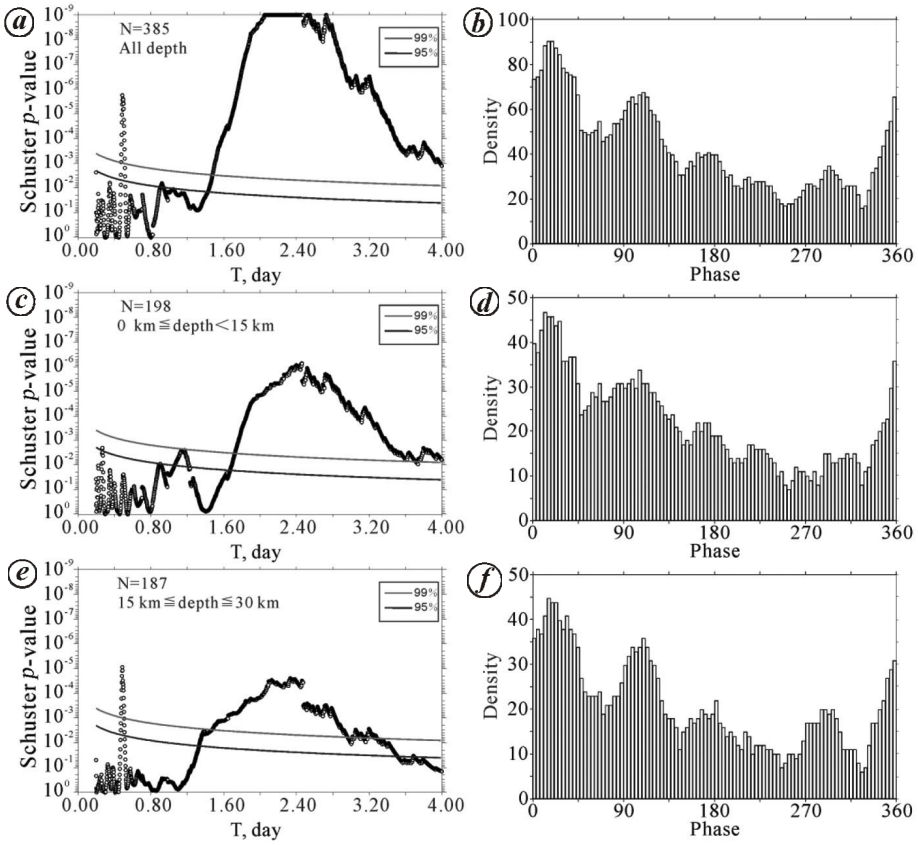

Figure 6. Schuster spectrum and phase variation curves 0–5 days after the mainshock for all depths (***a***, ***b***), set A (***c***, ***d***), and set B (***e***, ***f***). The period of the pulse series is 2 days and the pulse width is set to 0.2 days.

triggered by diurnal tides and deep earthquakes were triggered by semidiurnal tides in the Longmen Shan Fault.

The findings suggest that the tides may trigger an earthquake when pressure in the focal area is close to the critical level at which the earthquake occurs. Combining the Schuster spectrum and KORRECT methods may be feasible for detecting the latent tides.

1. Emter, D., Tidal triggering of earthquakes and volcanic events. In *Tidal Phenomena* (eds Wilhelm, H., Zürn, W. and Wenzel, H. G.), Lecture Notes in Earth Sciences, Springer, Berlin, Heidelberg, 1997, vol. 66; doi:10.1007/BFb0011468.
2. Berg, E., Triggering of the Alaskan earthquake of March 28, 1964, and major aftershocks by low ocean tide loads. *Nature* (*London*), 1966, **210**(5039), 893–896; doi:10.1038/210893a0.
3. Mohler, A. S., Earthquake/Earth tide correlation and other features of the Susanville, California, earthquake sequence of June–July 1976. *Bull. Seismol. Soc. Am.*, 1980, **70**, 1583–1593.
4. Tanaka, S., Tidal triggering of earthquakes precursory to the recent Sumatra megathrust earthquakes of 26 December 2004 (*M*w 9.0), 28 March 2005 (*M*w 8.6), and 12 September 2007 (*Mw* 8.5). *Geophys. Res. Lett*., 2010, **37**, L02301; doi:10.1029/2009GL041581.
5. Tanaka, S., Tidal triggering of earthquakes prior to the 2011 Tohoku-Oki earthquake (M_w 9.1). *Geophys. Res. Lett.*, 2012, **39**, L00G26; doi:10.1029/2012GL051179.
6. Chaodi, X., Xinglin, L., Xiaoyan, Z., Qingbo, M., Simeng, Y. and Yingnan, W., Tidal triggering of earthquakes in the Ning'er area of Yunnan Province, China. *J. Asian Earth Sci.*, 2017, **138**, 477–483; doi:10.1016/j.jseaes.2017.02.029.
7. Li, J. and Jiang, H., A statistical analysis on Wenchuan aftershock activity triggered by earth tide. *Earthquake Res. China*, 2011, **27**(4), 363–375 (in Chinese with English abstract).
8. Li, Q. and Xu, G. M., Tidal triggering of earthquakes in Longmen Shan region: the relation to the fold belt and basin structures. *Earth Planet Sp.*, 2012, **64**(9), 771–776; doi:10.5047/eps.2011.06.037.
9. Chen, D. and Yang, M., A study on tidal force triggering of the Wenchuan M_s 8.0 earthquake and its strong aftershocks. *Earthquake Res. China*, 2012, **26**(1), 87–96; doi:10.3969/j.issn.0891-4176.2012.01.007.
10. Ader, T. J. and Avouac, J. P., Detecting periodicities and declustering in earthquake catalogs using the Schuster spectrum, application to Himalayan seismicity. *Earth Planet. Sci. Lett.*, 2013, **377–378**, 97–105.
11. Kamal, M. L., The triggering of aftershocks by the free oscillations of the earth. *Bull. Seismol. Soc. Am.*, 1996, **86**(2), 299–305.
12. Huang, Y., Wu, J. P., Zhang, T. Z. and Zhang, D. N., Relocation of the *M* 8.0 Wenchuan earthquake and its aftershock sequence. *Sci. China* (*Series D*), 2008, **51**(12), 1703–1711.
13. Xu, X. *et al*., The M_S 8.0 Wenchuan earthquake surface ruptures and its seismogenic structure. *Seismol. Geol.*, 2008, **30**(3), 597–629 (in Chinese with English abstract)
14. Burchfiel, B. *et al*., A geological and geophysical context for the Wenchuan earthquake of 12 May 2008, Sichuan, People's

Republic of China. *GSA Today*, 2008, **18**(18), 4–11; doi:10.1130/GSATG18A.
15. Zhao, J. *et al.*, Spatio-temporal characteristics of strong aftershocks of the M_S 8.0 Wenchuan earthquake. *Earthquake Sci.*, 2010, **23**(3), 215–221.
16. Xie, C. D. *et al*., Pattern of stress change and its effect on seismicity rate caused by M_S 8.0 Wenchuan earthquake. *Sci. China Earth Sci*., 2010, **53**(9), 1260–1270.
17. Datta, A., Kamal, Triggering of aftershocks of the Japan 2011 Earthquake by Earth tides. *Curr. Sci.*, 2012, **102**(5), 792–796.
18. Dieterich, J. H., Nucleation and triggering of earthquake slip: effect of periodic stresses. *Tectonophysics*, 1987, **144**, 127–139.
19. Lockner, D. A. and Beeler, N. M., Premonitory slip and tidal triggering of earthquakes. *J. Geophys. Res*., 1999, **104**(B9), 20133–20151.
20. Beeler, N. M. and Lockner, D. A., Why earthquakes correlate weakly with the solid Earth tides: effects of periodic stress on the rate and probability of earthquake occurrence. *J. Geophys. Res.*, 2003, **108**(B8), 2391; doi:10.1029/2001JB001518.
21. Laurent, M. *et al*., Evidence of earthquake triggering by the solid earth tides. *Earth Planet. Sci. Lett.*, 2009, **278**(3–4), 0–375.
22. Zhang, P.-Z., Xu, X.-W., Wen, X.-Z. and Ran, Y.-K., Slip rates and recurrence intervals of the Longmen Shan active fault zone, and tectonic implications for the mechanism of the May 12 Wenchuan earthquake, 2008, Sichuan, China. *Chin. J. Geophys.*, 2008, **51**(4), 1066–1073; doi:10.3321/j.issn:0001-5733.2008.04.015 (in Chinese with English abstract).
23. Robert, A. *et al.*, Crustal structures in the area of the 2008 Sichuan Earthquake from seismologic and gravimetric data. *Tectonophysics*, 2010, 205–210.
24. Lu, R.-J., He, D.-F., John, S., Guan, S.-W., Ma, X.-M., Wang, M.-J. and Gui, B.-L., The discovery of structural wedges in the central Longmen Mountains front belt and its geometric and kinematic characteristics: Constraints on the dynamical mechanism of uplifting in the southeast margin of Qinghai Tibet Plateau. *Earth Sci. Front.*, 2010, **17**(5), 93–105 (in Chinese with English abstract).

ACKNOWLEDGEMENTS. Thanks for providing data of Wenchuan earthquake from Huang. This study was supported by the National Natural Science Foundation of China (Grant Nos.41964001, 41874156) and State Key Laboratory of Earthquake Dynamics (Project No. LED2019B04). We thank the associate editor and the anonymous reviewer for providing numerous comments that significantly improved the manuscript.

Received 19 September 2019; revised accepted 3 January 2020

doi: 10.18520/cs/v118/i8/1286-1292

Geochemical pathways of fluoride and boron in the alluvial aquifer of the Dwarka river basin, India

Raju Thapa[1], Srimanta Gupta[2,*] and Harjeet Kaur[1]

[1]Geo-Meteorological Risks Management Division, National Institute of Disaster Management, Ministry of Home Affairs, New Delhi 110 001, India
[2]Department of Environmental Science, The University of Burdwan, Burdwan 713 104, India

Dwarka river basin, situated in the Birbhum district of West Bengal, India is endemic to fluorosis as groundwater contains fluoride as high as 14 mg/L (permissible limit 1.5 mg/L). Co-existence of boron (B) and fluoride (F^{-1}) in groundwater, sometimes acts as a tool to predict the source of fluoride. This research was carried out with an objective to identify the geochemical relationship of these two elements and to find out their source(s) in groundwater. pH of groundwater of the study area was mostly neutral to alkaline, F^- generally ranged from 0.1 to 10.6 mg/L and boron ranged from 0.01 to 0.5 mg/L. Fluoride and boron showed a strong positive correlation indicating similar source. Fluorapatite observed in sediment samples was considered to be the main source of fluoride. Clay minerals found in the sediment sample were considered to be the most probable source of boron.

Keywords: Birbhum, boron, fluoride, fluoroapatite, groundwater, zeolite.

IN groundwater, occurrence of fluorine (F^-) and boron (B) together has attracted attention because of their effects on human health. Fluoride (F^{-1}) bearing minerals such as fluorite, cryolite and fluorapatite are commonly found in granitic rocks[1,2] which can contaminate groundwater with F^- through water–rock interaction. Occurrence of F^- has also been reported in secondary rocks such as argillaceous carbonate rocks[3], loess deposits[4], flood plain deposits[5,6]. Occurrence of F^- bearing minerals in hard rock terrains is well known, but F^- dynamics in alluvial terrains is less documented[7,8]. Natural sources of B include both igneous rocks and sedimentary deposits. The main process for the origin of B in groundwater is water–rock interaction in carbonate rocks, bentonites and evaporites, and ion exchange phenomenon of aquifer materials. In soil, B, associated with organically bound clay and mineral-fixed fractions commonly occurs as borates of sodium (Na) and calcium (Ca). In the earth's crust, average concentration of B is generally 10 ppm; its concentration in rocks ranges from 5 ppm in basalts to 100 ppm in shales[9]. Dwarka river basin (DRB) in Birbhum district

*For correspondence. (e-mail: srimantagupta@yahoo.co.in)